Three-dimensional space partition based on the first Laplacian eigenvalues in cells

O. Cybulski[1,*] and R. Hołyst[1,2,†]
[1]*Institute of Physical Chemistry, Polish Academy of Sciences, Kasprzaka 44/52, 01-224 Warsaw, Poland*
[2]*Department of Mathematics and Natural Science, Cardinal Stefan Wyszyński University, Dewajtis 5, 01-815 Warsaw, Poland*
(Received 17 March 2007; revised manuscript received 27 February 2008; published 8 May 2008)

We determine a partition of three-dimensional space into cells by minimization of the sum of the first Laplacian eigenvalues over the cells. This partitioning scheme emerges as a stationary state of a reaction-diffusion process taking place in a system of n different species which mutually annihilate, and simultaneously are duplicated in an autocatalytic reaction, so that the number of particles is kept constant and equal for each species. The system is considered in the limit of strong reactivity, so that the species separate each other into cells with well-defined, sharp boundaries. For a given n and fixed sizes of a periodic simulation box, this partition minimizes the aforementioned sum of eigenvalues. Further minimization is done by changing n and the side ratio of the periodic box. The global minimum is obtained for the structure with A15 symmetry, similar to the Weaire-Phelan foam. Depending on n and the side ratio, there are also many local minima, in particular: hcp (hexagonal close packed), fcc (face centered cubic), the Kelvin structure, and Frank-Kasper sigma phase.

DOI: 10.1103/PhysRevE.77.056101 PACS number(s): 82.40.Ck, 05.70.Ln, 83.80.Iz

I. INTRODUCTION

In our recent paper [1] we described a space partitioning scheme, given as the stationary state of a certain reaction-diffusion system. We discussed it in details for a two-dimensional system. In short, the system consists of n different species, each represented by the same number of particles, performing random walk within the accessible space. When two particles of the same type meet, nothing happens, but when they are of two different types, they mutually annihilite. The loss of particles due to the annihilation is immediately compensated by duplicating randomly chosen particles of the two types involved in the act of annihilation, so that the number of particles is preserved for each type separately. The process can be considered as the concurrence of diffusion, mutual annihilation, and autocatalytic reproduction of particles. These reactions lead to the spatial segregation of species. Dynamical and thermodynamical properties of the process were described in [2]. In the stationary state whole accessible space is divided into n adjacent domains, each occupied by only one type of particles. We have shown numerically [1,2] that this partition of the space satisfies the following variational rule, further referred to as the Σ_λ rule:

$$\sum_{i=1}^{n} \lambda_i = \text{minimum}, \tag{1}$$

where λ_i is the first (i.e., the smallest one) Dirichlet Laplacian eigenvalue of the ith cell, defined by the equation $\lambda_i p_i + \Delta p_i = 0$ with $p_i > 0$ in the interior and $p_i = 0$ at the boundary of the ith cell. Moreover, the spatial density of particles of ith type at point $\mathbf{r}$ is proportional to $p_i(\mathbf{r})$.

The goal of this paper is to find solutions of the Σ_λ rule in three-dimensional (3D) space and compare them with structures arising from other ways of partitioning space into cells. Two most widely known partitions are structure of foam and Voronoi tessellation for crystals. Kelvin studied the problem of foam consisting of equal volume cells characterized by the minimal total surface area. For this foam Kelvin proposed the structure composed of identical, slightly curved tetrakaidecahedra (14-hedra), located on the bcc lattice sites. A century after Kelvin, Weaire, and Phelan [3] found a structure with cells of two different types (12-hedra and 14-hedra of equal volume) with total area smaller by 0.33% than the Kelvin foam. There is no formal proof that the Wearie-Phelan structure is optimal and thus the Kelvin problem is still open.

In the two-dimensional case both the monodisperse foam [4] and the Σ_λ rule [1] led to the same structure: the periodic arrangement of the hexagonal cells. We are going to check if this similarity holds for 3D.

Space partitioning is also related to crystals, although the cells surrounding atoms must be extraneously constructed. This can be done using Voronoi tessellations. Although foams are often considered as relaxations of some Voronoi decompositions [5], the preferred structures of foams and crystals seem to be different. The Voronoi tessellation of fcc and hcp structure does not constitute a stable foam. On the other hand, the structure of Weaire-Phelan foam, conforming to Voronoi tessellation of A15 lattice (the symbol A15 comes from *Strukturbericht* designation [6]), occurs rarely in crystals, examples are β-tungsten and some alloys such as Cr_3-Fe.

The driving force behind the formation of the aforementioned structures is directly connected with the boundary of the cells in the case of foams, and with the interactions of their centers in crystals. Sometimes both interiors and boundaries of cells are important, as in self-organized structures formed by liquid crystalline micelles [7–9]. The new paradigm of space partitioning, defined by the Σ_λ rule, is related neither to the surface nor the central points, but spectral properties of cells.

*olgierd@ryba.ichf.edu.pl
†holyst@ptys.ichf.edu.pl

II. MODEL

Instead of the direct computation of the Laplacian eigenvalues in cells we use a continuous model of the aforementioned reaction-diffusion system in the limit of strong reactivity [2]. For each of n types we define the density function, $p_i(\mathbf{r},t)$, and starting from any distribution [but still p_i must be all non-negative, and at the given $\mathbf{r}$ only one $p_i(\mathbf{r})$ may be nonzero] we look for the stationary state by solving the following integrodifferential equations:

$$\frac{\partial}{\partial t}p_i = D\Delta p_i + \Lambda_i(t)p_i, \tag{2}$$

$$\int_V p_i dV = 1, \tag{3}$$

$$p_i p_j = 0 \quad (i,j = 1, \ldots, n,\ i \neq j), \tag{4}$$

where D is the diffusion constant (the same for each component) and $\Lambda_i(t)$ are the time dependent Lagrangian multipliers, which can be unambiguously determined to reconcile the evolution, Eq. (2), with the normalization, Eq. (3), and the free boundary condition describing annihilation, Eq. (4). Physically, the last term in Eq. (2) describes how many particles are duplicated at a given point and time. In the stationary state, each p_i becomes the first eigenfunction of the Laplacian with Dirichlet boundary conditions, so that

$$\lambda_i p_i + \Delta p_i = 0, \tag{5}$$

where λ_i is the first eigenvalue of the cell occupied by the ith component.

Beyond the stationary state, both the boundaries of cells and p_i do change in time. As long as the evolution proceeds, p_i do not conform to the eigenfunctions of cells in their momentary shapes. However, there exist a variational rule that sets the arrow of time. We have shown [1,2,10] the existence of the positively defined functional:

$$\sigma[p_1, \ldots, p_n] = -\sum_{i=1}^{n}\left(\int_V p_i \Delta p_i dV\right)\left(\int_V p_i^2 dV\right)^{-1}, \tag{6}$$

which monotonously decreases in time until it reaches a minimum in the stationary state. In the stationary state the sum of λ_i is minimized as well [Eq. (1)] and, moreover, $\Sigma\lambda_i = \sigma$. In order to compare structures for different geometries (X,Y,Z) and different n we renormalize σ as follows:

$$\tilde{\sigma} = \frac{(XYZ)^{2/3}}{n^{5/3}}\sigma. \tag{7}$$

The renormalized $\tilde{\sigma}$ does not depend on the overall scale. In the stationary state (but not beside it) $\tilde{\sigma}$ can be expressed in terms of average properties of cells:

$$\tilde{\sigma} = \bar{V}^{2/3}\bar{\lambda}, \tag{8}$$

where $\bar{V} = XYZ/n$ is the average volume of a cell and $\bar{\lambda} = (\lambda_1 + \lambda_2 + \cdots + \lambda_n)/n$ is the average first eigenvalue of a cell in the partition. The analogous cost function for monodisperse foams [11] is often chosen in the form $\mu = \bar{A}^3/V^2$ where $\bar{A}$ is the average area surface of a cell and $V = \bar{V}$ since all V_i are equal. Both $\tilde{\sigma}$ and μ are functions of $[n,X,Y,Z]$, and both may be used to classify different structures for the sake of optimality; in both cases the lower the value, the better the structure.

III. METHOD OF SIMULATION

Although we are interested only in the stationary state, the way of its finding is nothing but simulation of the dynamic process described above, starting from any initial conditions (random or strictly prepared as well), and eventually reaching the stationary state (not necessarily unique). The simulation is performed using discrete space and time. Instead of the continuous $p_i(\mathbf{r},t)$, the density of the ith component is represented by $p^i_{h,k,l}$ with h,k,l indicating a node of the regular periodic grid (time index was omitted for brevity). The simulation method belongs to the family of fractional step methods, also known as operator splitting. A complete time step of the simulation relies on a single repetition of the following cycle.

(A) Diffusion step.
(B) Annihilation step.
(C) Renormalization step.

For clarity, results of intermediate calculations after these steps are denoted p', p'', and p''', respectively. In fact, there is only one data structure. Moreover, there is no need to store n separated densities for different components—an efficient algorithm should store only two numbers per node: the common density value and the integer number determining the current component.

A. Diffusion step

For all lattice nodes the density functions are treated by the diffusion operator as follows:

$$p'^i_{h,k,l} = p^i_{h,k,l} + D\Delta_{h,k,l}p^i, \tag{9}$$

where $\Delta_{h,k,l}p^i$ stands for the discrete Laplacian of the second order. After this step, the lattice nodes lying along the interface are shared between two or more components.

B. Annihilation step

For such a node (h,k,l), which has been distributed between several components as a result of diffusion step, we determine the surviving component, i, and its new density, p^i, whereas the remaining p^j for $j \neq i$ are reset to 0. The choice of i and the calculation of p^i is performed by modeling a chemical reactor, in which the homogeneous mixture of n components undergoes the reaction of mutual annihilation between components. Details of this procedure are described in [2], whereas its effective use is described hereafter.

The component i, which remains in the reactor as the result of full exhaustion of all other reagents, is appointed as the one for which the concentration at the tested node has been the largest:

$$i{:}p'^{i}_{h,k,l} = \max\{p'^{1}_{h,k,l}, \ldots, p'^{n}_{h,k,l}\}. \tag{10}$$

The new density is calculated as follows:

$$p''^{i}_{h,k,l} = (p'^{i}_{h,k,l})^{2-n} \prod_{j=1,\ldots,n,\ j\neq i} (p'^{i}_{h,k,l} - p'^{j}_{h,k,l}). \tag{11}$$

If two or more largest density functions have been equal, then there is no winner—all densities $p''^{1}_{h,k,l}, p''^{2}_{h,k,l}, \ldots, p''^{n}_{h,k,l}$ are reset to 0, which means that the node becomes empty. Obviously, the annihilation step does not change nodes which have been occupied by only one component after the diffusion step: for such nodes $p''=p'$.

C. Renormalization step

In Eq. (2), the loss of normalization is immediately compensated by the term $\Lambda_i(t)p_i$. Here, however, the renormalization is performed as follows:

$$W_i = \sum_{h,k,l} p''^{i}_{h,k,l}, \tag{12}$$

$$p'''^{i}_{h,k,l} = \frac{1}{W_i} p''^{i}_{h,k,l}. \tag{13}$$

After this procedure, the full time step is completed—p'''^{i} will be used as p^i in the next time step.

D. Testing the algorithm

The justification for splitting of the right side of the differential equation such as Eq. (2) into separate operations of diffusion, annihilation, and renormalization, as well as numerical errors introduced by this trick, were discussed in our previous paper [10] for the case of $n=1$ and a constant, absorbing boundary condition.

However, for $n>1$ it is not easy to determine errors produced by the annihilation procedure described above. A detailed discussion of the problem is presented in the Appendix. Regardless of whether the evolution of boundaries in simulations conforms to the continuous model defined by Eqs. (2)–(4), regardless of any dynamical properties of both the continuous and discrete systems, there is one strong argument in favor of the method: the discrete version of the functional $\tilde{\sigma}$, defined in Eq. (7), systematically decreases until the stationary state is reached. This means that even if the algorithm does not exactly follow the dynamics given by Eqs. (2)–(4), it goes in the right direction, most probably leading to the same local minimum of $\tilde{\sigma}$, or, to be more precise, its discrete equivalent:

$$\tilde{\sigma} = -\frac{(XYZ)^{2/3}}{n^{5/3}} \sum_{i=1}^{n} \frac{\sum_{h=1}^{X}\sum_{k=1}^{Y}\sum_{l=1}^{Z} (p^{i}_{h,k,l}\Delta_{h,k,l}p^{i})}{\sum_{h=1}^{X}\sum_{k=1}^{Y}\sum_{l=1}^{Z} (p^{i}_{h,k,l})^2}. \tag{14}$$

In order to monitor simulations, the above functional was calculated with $\Delta_{h,k,l}$ being the discrete Laplacian operator of the second order—the same that was used in the diffusion step.

However, in order to improve the accuracy in some special cases (see the Appendix), the final results for $\tilde{\sigma}$ in the stationary state were calculated using a 25-point, eight order Laplacian [16] and a kind of extrapolation of p^i onto the nodes occupied by components other than i. If such nodes, say, of the type j instead of i, belong to the 3D 24-point neighborhood of $\{h,k,l\}$ (e.g., nodes in the range from $\{h-4,k,l\}$ to $\{h-1,k,l\}$ and further from $\{h+1,k,l\}$ to $\{h+4,k,l\}$), then $-p^j$ is used instead of $p^i(=0)$ as the local density at these nodes.

Formally, this improvement may be written as follows:

$$\tilde{\sigma} = -\frac{(XYZ)^{2/3}}{n^{5/3}} \sum_{i=1}^{n} \frac{\sum_{h,k,l}\left[p^{i}_{h,k,l}\Delta_{h,k,l}(p^{i} - \sum_{j\neq i} p^{j})\right]}{\sum_{h,k,l} (p^{i}_{h,k,l})^2}. \tag{15}$$

The discussion of this pseudoextrapolation has been presented in [2], whereas the comparison of results for two- and eight-order Laplacians is given in the Appendix.

One might question the use of an eight-order differential operator in connection with the simplest possible method of numerical integration (the rectangular quadrature). This doubt would be justified for an arbitrary function, but not for p^i in the stationary state. In particular, if p^i is exactly an eigenfunction of the Laplacian, the choice of quadrature does not matter—as long as the same quadrature is used in the numerator and denominator of Eqs. (6) and (14).

IV. RESULTS

More than 1000 coarse simulations, performed with periodic boundary conditions for various $[n,X,Y,Z]$, enabled us to select interesting ranges of the parameters for final simulations with a grid refined up to $X=Y=Z=300$ nodes. The simulations were performed until the system reached the stationary state, starting from both random and symmetric initial conditions. The former required much more simulation time and always led to stable structures, whereas the latter created the possibility of getting stuck in unstable stationary states, which could be an advantage when ranking both stable and unstable structures by $\tilde{\sigma}$.

Figure 1 shows the cells (estimated as the zero density isosurfaces) for the parameters $[n,X,Y,Z]$ chosen as to enable four basic structures of crystallography: fcc (denoted by *strukturbericht* designation A1, see [6]), bcc (A2), hcp (A3), and diamond lattice (A4). Structures A1–A3 are stable and optimal in their geometries (the parameters and resulting $\tilde{\sigma}$ are collected in Table I) whereas A4 is unstable i.e., any perturbation of densities will lead to a new structure. The cells of A1 and A3 are dodecahedra with all flat faces: 12 identical rhombs in A1 and six rhombs and six trapezoids in A3. After rotation of the marked half by 60°, the A1 cell transforms into A3. Due to this symmetry, A1 and A3 structures have equal surface area and would be equivalent as foams (in terms of cost function μ); but they are not equivalent with respect to Σ_λ minima, since their values of $\tilde{\sigma}$ are slightly different, in favor of A3. Cells of A2 and A4 have both flat and curved faces: six flat and eight curved in the

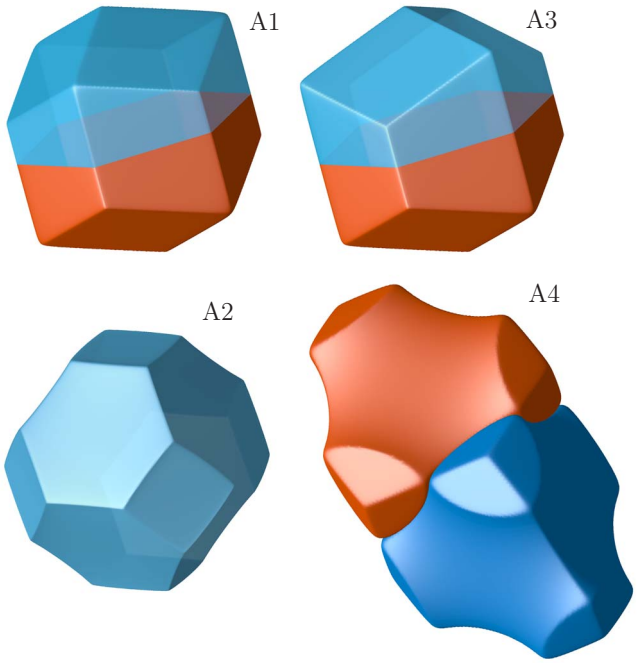

FIG. 1. (Color online) Single cells of A1 (fcc), A2 (bcc), A3 (hcp), and two adjacent cells of unstable A4 (diamond) structure.

tetrakaidecahedron of A2, and 12 flat and four curved in the hexakaidecahedron of the unstable A4 structure. The A2 cell looks very much like Kelvin solid, but the details of curvature (Fig. 2) may be different. In contradistinction to foams, A2 structure is far from being optimal in the partition minimizing $\tilde{\sigma}$—we found several better structures, including A3 and A1 (Table I).

Surprisingly the best structure, in terms of both the surface area and the functional $\tilde{\sigma}$, is A15 structure, whose translational unit is a cube ($X=Y=Z$) consisting of $n=8$ cells of two different shapes: two dodecahedra and six tetrakaidecahedra, as shown in two different views in Fig. 3. Let us suppose the periodic box with $X=Y=Z=4$. The centers of

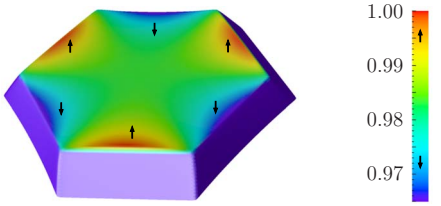

FIG. 2. (Color online) Curvature of hexagonal face in cell of A2. "Square" faces of the same cell are flat.

cells are at points with coordinates [0,0,0] and [2,2,2] for 12-hedra and [0,2,1], [0,2,3], [1,0,2], [3,0,2], [2,1,0], and [2,3,0] for 14-hedra. As shown in Fig. 4, there are two types of vertices in 12-hedron and four types in 14-hedron. Vertices of one such 12-hedron are

$\bigcirc$ $[\pm a, \pm a, \pm a]$ (eight vertices in Fig. 4),

$\lhd$ $[0, \pm b, \pm c]$, $[\pm b, \pm c, 0]$, $[\pm c, 0, \pm b]$ $(12\times)$

and of one of 14-hedra (shifted to the origin):

$\bigstar$ $[(1-a), \pm(2-a), \pm a]$, $[-(1-a), \pm a, \pm(2-a)]; (8\times)$,

$\diamond$ $[(1-c), \pm(2-b), 0]$, $[-(1-c), 0, \pm(2-b)]$; $(4\times)$,

$\rhd$ $[1, \pm(2-c), \pm b]$, $[-1, \pm b, \pm(2-c)]$; $(8\times)$,

$\triangledown$ $[1, 0, \pm 1]$, $[-1, \pm 1, 0]$ $(4\times)$.

Parameters a, b, and c describe a general structure with A15 symmetry. According to the previous study of A15 foam structure [11], these parameters are $c=\sqrt[3]{2}\approx 1.259\,92$, $b=c/2\approx 0.629\,96$, $a=(2/3)c\approx 0.839\,95$ for flat faces. The values obtained from our simulations are slightly different:

TABLE I. Numbers of different polyhedra (12–16 faces) and optimal geometries of selected structures sorted by $\tilde{\sigma}$ [estimated from Eq. (15) with an absolute error less than 10^{-3}]. Unstable structures A_h and A4 were obtained only due to the symmetry of initial conditions.

	Composition (polyhedra)						Geometry		
Structure	n	#12	#13	#14	#15	#16	Y/X	Z/X	$\tilde{\sigma}$
A15	8	2	-	6	-	-	1	1	26.9722
A3	8	8	-	-	-	-	$\sqrt{\frac{3}{4}}$	$\sqrt{\frac{2}{3}}$	26.9756
A1	4	4	-	-	-	-	1	1	26.9763
A_b	30	2+8	-	8+8	4	-	1	$\sqrt{2-\sqrt{3}}$	26.9828
Shields	52	12	12	12+12	4	-	$\sqrt{3}$	$\sqrt{2-\sqrt{3}}$	26.9953
A2	16	-	-	16	-	-	1	1	27.0303
Rhombs	24	-	8+8	8	-	-	1	$\sqrt{\frac{1}{3}}$	27.0952
Z	14	6	-	4	4	-	$\sqrt{3}$	1	27.1140
C15	24	16	-	-	-	8	1	1	27.2195
A_h	8		⋯	⋯ cubes ⋯	⋯		1	1	29.6088
A4	8	-	-	-	-	8	1	1	33.4450

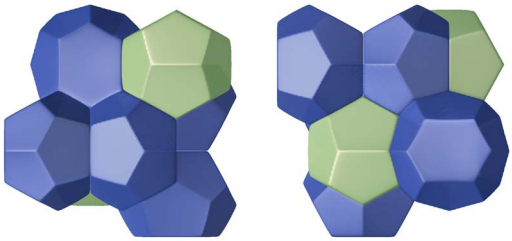

FIG. 3. (Color online) Translational unit of A15 structure with both dodecahedra marked by green (lighter gray shade).

$c \approx 1.260$, $b \approx 0.591$, $a \approx 0.814$. This fact means that, although similar, A15 structure resulted from the Σ_λ rule is slightly different than the Weaire-Phelan foam [11]. Apart from the different vertices, also the curvature of the faces differs, as well as 14-hedron to 12-hedron volume ratio, which is about 1.054 in Σ_λ A15 and 1 (by definition) in the foam. The angle of meeting edges in foam [11], $\arccos(-1/3) \approx 109.47°$, is close to the angle of the regular pentagon, 108°. For this reason, the dodecahedron in the A15 structure is similar to the regular dodecahedron. The difference can be seen when trying to overlap two such dodecahedra after rotation of one of them by 72°, as shown on the right side in Fig. 5. Thanks to the curvature of faces, this dodecahedron is a strictly convex solid.

A15 belongs to the family of tetrahedrally close packed (TCP) structures which often occur in monodisperse foams. Some of them are called Friauf-Laves or Frank-Kasper phases [12]. Many of such structures can be assembled from basic building blocks of several types [13], as illustrated in Fig. 6. Using the marked atom positions as the initial density peaks leads to the formation of the appropriate structure, e.g., as shown in Fig. 7 for the Frank-Kasper σ phase, with *strukturbericht* designation A_b. Information about the structures from Fig. 6 as well as previously described A1–A4 and (not shown) Laves cubic phase with *strukturbericht* designation C15 are collected in Table I. From columns #12–#16 one can read numbers of different kinds of polyhedra per rectangular prism with sides X,Y,Z (a single translational unit in the periodic structure). For example, A_b consists of ten 12-hedra of two different kinds (2+8), 16 14-hedra of two kinds (8+8), and four identical 16-hedra enclosed in the periodic box of size $d \times d \times \sqrt{2-\sqrt{3}}d$.

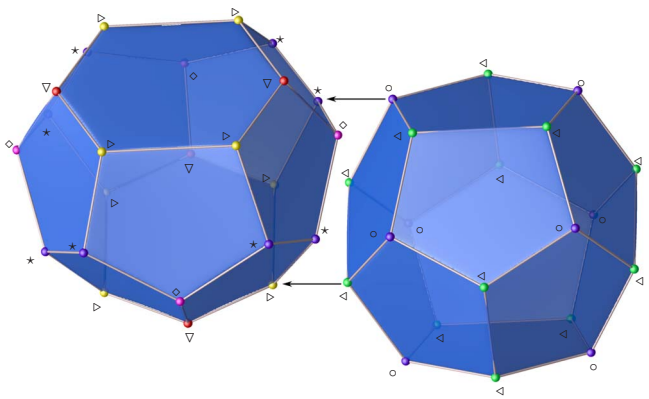

FIG. 4. (Color online) Dodecahedron (left) together with adjacent tetrakaidecahedron (right) of A15 structure with different types of vertices marked.

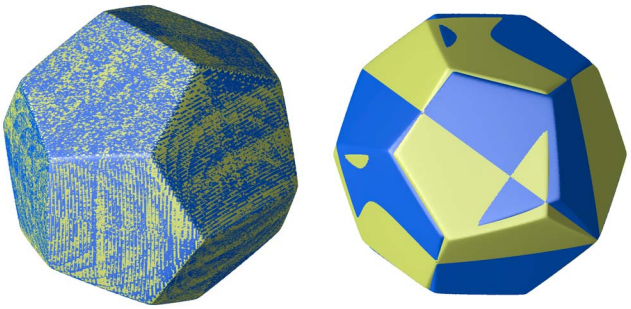

FIG. 5. (Color online) Overlapping two colored (two different gray levels) A15 dodecahedra after rotation of one of them by 120° around the threefold axis, and by 72° around presumed fivefold axis of symmetry (the axis in both cases points outward perpendicularly to the drawing plane). Clearly this dodecahedron has a threefold symmetry axis but lacks the fivefold symmetry axis.

V. SUMMARY

We introduced a paradigm of 3D space partitioning, the $\Sigma\lambda$ rule, and proposed a scale-independent functional, $\tilde{\sigma}$, to classify its solutions. On the basis of computer simulations we also found several minima and classified them in term of $\tilde{\sigma}$.

The lowest value, $\tilde{\sigma} \approx 26.9722$, was obtained for A15 structure. If 3D space could be tessellated by spheres, their $\tilde{\sigma}$ would be equal to $(\frac{4}{3})^{2/3}\pi^{8/3} \approx 25.6463$. Optimality of the

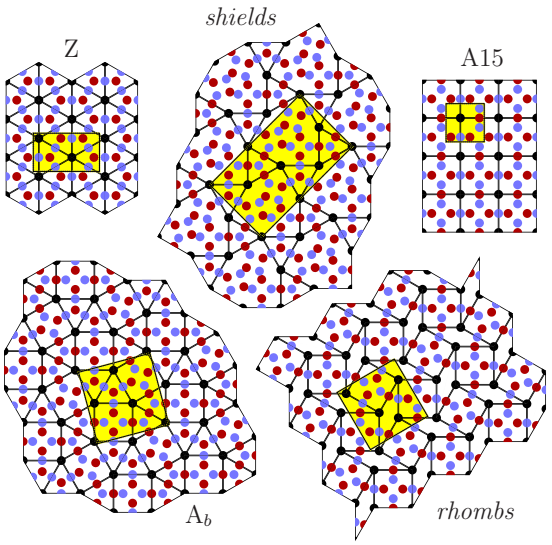

FIG. 6. (Color online) TCP (tetrahedrally closed packed) structures assembled from blocks of several types. They are: Z, A15, σ (A_b), *shields*, and *rhombs*. Circles denote atom locations along the Z axis, perpendicular to the drawing plane: circles within blocks are at $z=k$ and $z=k+1/2$ (distinguished by two different colors / gray levels), black circles in corners of blocks are at $z=k\pm 1/4$ for any integer k. Highlighted are periodic units, whose height along the Z axis is 1, the same as the side length of the square block.

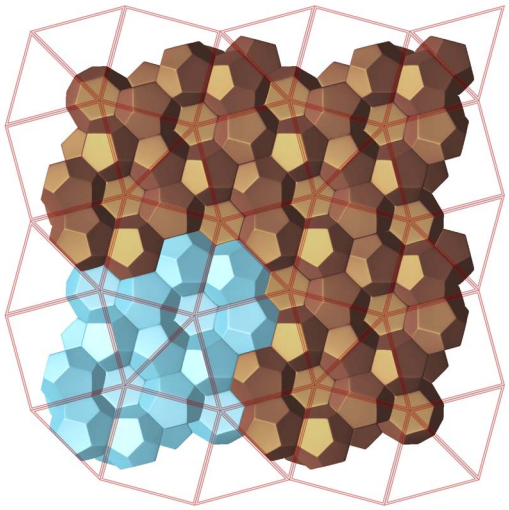

FIG. 7. (Color online) Four adjacent translational units of A_b structure (in the crystallography known as the Frank-Kasper σ phase). One such unit (highlighted) contains $n=30$ cells. Lines enable identification of triangular and square blocks corresponding to the initial configuration from Fig. 6.

A15 structure both here and in the ideal foam suggests that A15 cells are most similar to a sphere—the ideal shape of a single cell as abstracted from the rest of the partition. There are counterexamples, however, in other paradigms of space partitioning, where also a sphere is a transcendent ideal, but the best realization is not the Weaire-Phelan structure. In theory of vector quantizers [14] what is minimized is the effective normalized moment of inertia (NMI). In this case the optimal structure is A2 and not A15.

The Laplacian is one of the most prominent operators and we believe that the space partition based on its spectral properties constitutes a valuable paradigm in physics. The Σ_λ rule may occur in various different optimization problems. The sum of ground state energies of quantum wells filling the space will be minimized by satisfying the Σ_λ rule. The same partition should be considered when minimizing the mean escape rate (in the sense of reaching the walls) of randomly walking particles enclosed in the cellular structure.

ACKNOWLEDGMENTS

This work was supported as a scientific project during 2006 to 2007 and also ESF program SONS (SCALES) 2006–2009 by the Polish Ministry of Science and Higher Education. R.H. acknowledges support from the Foundation for Polish Science (Grant "Mistrz").

APPENDIX: TESTS OF NUMERICAL CALCULATIONS

The problem we tried to solve belongs to the family of so-called free boundary problems, which in general are hard to deal with, especially in terms of error analysis. These errors are not only due to discretization and use of a finite grid, but also due to the uncertainty of estimated boundary, whose evolution emerges as a result of simulation. One of the most available methods for testing numerical algorithms is checking solutions, which are known analytically, or may be obtained in several different ways. Hereby we present two such tests.

1. Analytical results for $n=2$

Due to the periodic boundary conditions, use of $n=2$ corresponds to the partitioning of space into two continuous structures of infinite size rather than into infinitely many clones of two closed cells. For this reason the interpretation of $\tilde{\sigma}$ given by Eq. (7) does not make sense for the case of $n=2$. However, simulations performed for this case may be compared to analytical results, which are known [15]. For $X=Y=Z$, i.e., for a cubic box, the interface conforms to the nodal surface of the function:

$$Q(x,y,z) = A\,\sin\frac{2\pi x+\alpha}{X} + B\,\sin\frac{2\pi y+\beta}{X} + C\,\sin\frac{2\pi z+\gamma}{X}$$

defined by $Q(x,y,z)=0$. The density functions, $p_1(\mathbf{r})$ and $p_2(\mathbf{r})$, correspond to the positive and negative part of $Q(\mathbf{r})$, so that

$$p_1(\mathbf{r}) = Q(\mathbf{r}),\ \ p_2(\mathbf{r}) = 0 \quad [\text{for}\ \ Q(\mathbf{r}) > 0],$$

$$p_1(\mathbf{r}) = 0,\ \ p_2(\mathbf{r}) = -Q(\mathbf{r}) \quad [\text{for}\ \ Q(\mathbf{r}) < 0].$$

Parameters A, B, C, x_0, y_0, and z_0 are arbitrary, though at least one of (A,B,C) must be nonzero, and there must be

$$\int_0^X \int_0^X \int_0^X |Q(x,y,z)|dx\ \ dy\ \ dz = 2$$

to normalize p_1 and p_2. Depending on the initial conditions of simulation, different combinations of these six constants (five of them independent) may be needed to reconstruct the resulting stationary state. Such a degeneracy is due to symmetry of the cube and may be used for testing quality of simulations. First of all, as long as the fluctuations are not taken into account, there should not be any evolution from a stationary state toward another one, with different parameters. Second, each of the stationary states must have the same value of $\tilde{\sigma}$. Third, up to the numerical errors, the calculated $\tilde{\sigma}$ must be equal to the theoretical value, $2^{4/3}\pi^2 \approx 24.869\,844\,678\,135$.

These three properties were tested for simulations starting from a random initial condition with varying seed. Several grids were used: from $10\times10\times10$ up to $80\times80\times80$ nodes. Values of $\tilde{\sigma}$ calculated with the second-order discrete Laplacian were: 24.0624 for $X=10$, 24.8188 for $X=40$, and 24.8571 for $X=80$ (X denotes grid—number of nodes per dimension). The same values calculated with eight-order Laplacian were 24.869 67 for $X=10$, 24.869 844 675 for $X=40$, and 24.869 844 678 12 for $X=80$. It is clear that the deviations from the theoretical value of $\tilde{\sigma}$ are solely due to the truncation error of discrete Laplacian, and are of the order of $(X/2)^{-2}$ for second-order Laplacian, and $(X/2)^{-8}$ for eight-order Laplacian (relative errors, estimated for the minimum number of width of the single component domain, which is $X/2$ as in the case of two parallel stripes shown in Fig. 8).

No dependence on initial conditions was observed, even though fitted values of A, B, C, x_0, y_0, and z_0 covered the

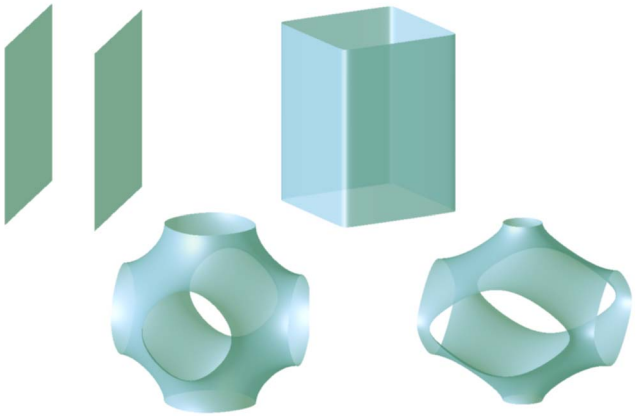

FIG. 8. (Color online) Triply periodic surface dividing two infinite domains ($n=2$), depending on the parameters: $A\neq 0$, $B=C=0$ (upper left), $A=B\neq 0$, $C=0$ (upper right), $A=B=C\neq 0$ (bottom right), each nonzero, no two equal (bottom right)

whole available range. Moreover, any deviations of the stationary densities p_1 and p_2 from the exact solution (constructed with these fitted parameters and measured at grid nodes) were of the order of floating point arithmetic error (10^{-15} here). This is because the continuous and the discrete eigenfunctions of the Laplace operator for a rectangular prism are strictly coincident, as far as the grid is regular and oriented in accordance with the edges of the prism.

2. Simple cubic structure

For the reason mentioned above, metastable structures based on simple cubic lattice, *strukturbericht* designation A_h, result in very accurate $\tilde{\sigma}$, as far as the orientation of the lattice (more precisely: the set of initial conditions in the form of a lattice of n evenly spaced density peaks) is compatible with the simulation grid and the periodic boundary conditions. For example, calculations of $\tilde{\sigma}$ with eight-order discrete Laplacian produce the same result for ($X=Y=Z=128$, $n=512$) as for ($X=Y=Z=32$, $n=8$), since in both cases the domains of single component are the same cubes of size $16\times 16\times 16$. For such a cube the relative error for eight-order Laplacian should be of the order of $16^{-8}\approx 2\times 10^{-10}$. The calculated $\tilde{\sigma}=29.608\,813\,18$ whereas the exact value is $3\pi^2\approx 29.608\,813\,20$, thus the relative difference is of the same order as the truncation error of the Laplacian.

3. Slanted simple cubic structure for $n=24$

In the two latter examples the overall errors involving calculation of $\tilde{\sigma}$ were exceptionally small, due to the coincidence of discrete and continuous eigenfunctions of the problem. As a counterexample, we again consider the unstable A_h (simple cubic) structure, but this time the main crystallographic axes of the structure are not parallel to the axes of the simulation grid.

Consider a rectangular prism of size $\sqrt{8}\times\sqrt{6}\times\sqrt{12}$. It has volume 24, and may be used as a unit cell encapsulating 24 atoms of a simple cubic structure with lattice constant equal to 1. The positions of atoms may be expressed as $h\mathbf{B_1}+k\mathbf{B_2}+l\mathbf{B_3}$, where h,k,l are integer numbers, and the vectors:

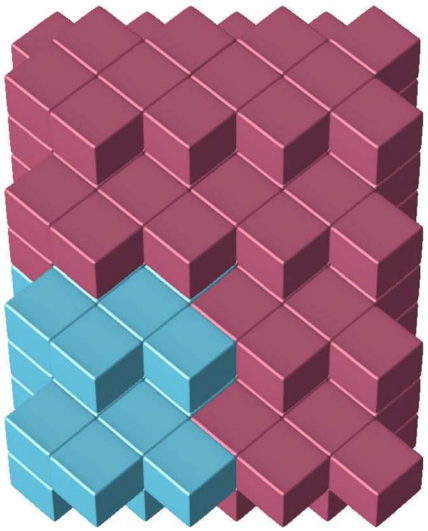

FIG. 9. (Color online) Simple cubic (A_h) structure slanted toward the axes of the periodic box. Four adjacent unit cells are shown. The Z axis of the simulation box is perpendicular to the picture's plane, so that the inclination of the "crystallographic planes" is clear.

$$\mathbf{B_1}=\left[\frac{\sqrt{2}}{2},\ \frac{\sqrt{6}}{6},\ \frac{\sqrt{3}}{3}\right],$$

$$\mathbf{B_2}=\left[-\frac{\sqrt{2}}{2},\ \frac{\sqrt{6}}{6},\ \frac{\sqrt{3}}{3}\right],$$

$$\mathbf{B_3}=\left[0,\ \frac{2\sqrt{6}}{6},\ -\frac{\sqrt{3}}{3}\right]$$

form the orthonormal basis, i.e., they are mutually perpendicular and of unit length.

Unfortunately, such a construction, even scaled, cannot be realized with a regular grid—the side ratios are irrational. However, an approximation may be used. We used $X=132$, $Y=114$, $Z=162$, and generated the initial density peaks at the grid nodes pointed by an integer multiple of the vectors:

$$\mathbf{B_1}=[33,19,27],$$

$$\mathbf{B_2}=[-33,19,27],$$

$$\mathbf{B_3}=[0,38,-27].$$

During the simulation the metastability of A_h was clearly seen—the functional $\tilde{\sigma}$ given by Eq. (14) decreased rapidly to some metastable value, and after a long time of very slow descent, continued to decrease toward its new (probably stable) stationary state. In the plateau (for the point of the slowest descent) there was $\tilde{\sigma}=29.6079$, and the obtained structure is given in Fig. 9. A deviation from the theoretical value of $\tilde{\sigma}=3\pi^2$ is partly due to rounding of X,Y,Z, but also

may be caused by the simulation method. Let us assume it is caused by the truncation error of the second order discrete Laplacian. For the cubes of size $d=(XYZ/n)^{1/3}\approx 47$ the relative error should be of the order of $d^{-2}\approx 5\times 10^{-4}$, that is about ten times larger than the observed (relative) difference.

4. Conclusions

Summarizing the above-mentioned cases and many other similar tests made for a two-dimensional prototype of the algorithm [1], we conjecture that the maximum relative error of estimating $\tilde{\sigma}$ may be assumed as $(XYZ/n)^{-2/3}$. In order to improve the accuracy without dealing with very long times of simulation we used the mesh refining—the structures found for (X,Y,Z) were mapped onto (kX,kY,kZ), most often with $k=2$ or 3. After refining, the simulation was performed up to the new stationary state, which was indicated by tracing the evolution of the functional $\tilde{\sigma}$.

[1] O. Cybulski and R. Holyst, Phys. Rev. Lett. **95**, 088304 (2005).
[2] O. Cybulski, V. Babin, and R. Holyst, Phys. Rev. E **71**, 046130 (2005).
[3] D. Weaire and R. Phelan, Philos. Mag. Lett. **69**, 107 (1994).
[4] T. C. Hales, Discrete. Comput. Geom. **25**, 1 (2001).
[5] A. M. Kraynik, D. A. Reinelt, and F. van Swol, Phys. Rev. E **67**, 031403 (2003).
[6] *Strukturbericht* designation is a partly systematic atlas of the crystalographic structures, introduced by P. P. Ewald and C. Herman, in *Strukturbericht*, Vol. I (1913–1928), at present maintained by http://cst-www.nrl.navy.mil/lattice/struk/.
[7] G. Ungar *et al.*, Science **299**, 1208 (2003).
[8] G. Ungar and X. B. Zeng, Soft Mater. **1**, 95 (2005).
[9] P. Ziherl and R. D. Kamien, Phys. Rev. Lett. **85**, 3528 (2000).
[10] O. Cybulski, V. Babin, and R. Holyst, Phys. Rev. E **69**, 016110 (2004).
[11] R. Kusner and J. M. Sullivan, Forma **11**, 233 (1996).
[12] F. C. Frank and J. S. Kasper, Acta Crystallogr. **12**, 483 (1959).
[13] J. Roth and A. R. Denton, Phys. Rev. E **61**, 6845 (2000).
[14] N. Kashyap and D. L. Neuhoff, IEEE Trans. Inf. Theory **47**, 2538 (2001).
[15] O. Cybulski, D. Matysiak, V. Babin, and R. Holyst, J. Chem. Phys. **122**, 174105 (2005).
[16] T. Beck, J. Comput. Chem. **20**, 1731 (1999).